Using of Satellite-Based Rainfall Estimates to Monitor Flash Floods in Wadi Araba Region Western Suez Gulf

***Dr. Hany Rabie Nady Mohamed* (*)**

Abstract:

Satellite imagery provides significant data reliable to study weather and climate elements through frequent observation for these elements using remote sensing systems that care about such researches, like NOAA satellite which is considered the oldest climate remote sensing system. Satellites resemble clues to mathematical models so as to define pressure distribution, temperature thickness and density of atmosphere layers, calculating wind movement indirectly by measuring cloud movement from fixed satellites, as well as using telescopes with high capacity in both visual and thermal fields, as it records temperature gradation within cloud layers, comparing them and conclude simple primary results. This research depended on data from The Precipitation Estimation from Remotely Sensed Information using Artificial Neural Networks (PERSIANN) project under California University meteorological, hydrological and remote sensing observation center which acts upon extracting rainfall data from satellite imagery using Neural Network Models where data are available in four patterns among which the data type PERSIAN CCS has been relied upon being a highly accurate spatial data where cell dimensions reach 4 km × 4 km. Research period extended between (2015 – 2021). During this period these digital files have been analyzed and modelled for purpose of defining spatial and time variations in rainfall expected along the study period and its impacts in flash floods in the study area basins. The study revealed fluctuating rainfall patterns, with an average of 19.85 mm in 2018 and 3.83 mm in 2020. Spring received the highest rainfall, with 17.22 mm, followed by winter at 14.89 mm. March had the highest rainfall, with 19.2 m, followed by December at 17.7 m. Flash Floods volume in Wadi Arba ranged from 200 million m^3 in 2018 and 2019 to 10.41 million m^3 in 2015.

Keywords: Rainfall Estimations – Satellite images – PERSIANN **-** Flash Floods – Wadi Araba.

(*) Geography and GIS department, Beni Suef University.

Introduction:

Precipitation, a crucial meteorological and hydrological element, provides accurate information on global water changes, aiding in meteorological and hydrological monitoring and forecasting, enhancing disaster response capabilities and optimizing water resource management, (Michaelides, S. et al., 2009) (Kavetski, D, et al., 2006) (Ebert, E, et al., 2007). Global locations often lack sufficient precipitation observing networks for effective water resource management, climate analysis, and natural hazard mitigation, especially in complex terrain regions with sparse infrastructure. Rain gauge measurements may not accurately characterize spatial patterns, and the distribution of gauges is biased towards areas with coexisting infrastructure, (Hong, Y., et al. 2007). Precipitation is vital for Earth's hydrologic cycle, affecting water and energy balance, and accurate observation enhances climate resilience, aids infrastructure design, and aids early warning systems. It also aids in understanding Earth's climate, enabling forecasting and strategic planning on water supply issues. Real-time precipitation data is essential for disaster management planning, (Nguyen, P., et al. 2018).

Satellite techniques for precipitation estimation utilize data from geostationary Earth orbiting (GEO) and low Earth orbiting (LEO) satellites, providing images every 5-30 minutes and passive microwave information about hydrometeors. Early efforts involved analyzing individual pixel information and cloud image types. The Tropical Rainfall Measurement Mission (TRMM) in 1997 marked a significant advancement in operational satellite-based precipitation products. The 2018 GPM mission, launched with multiple passive microwave sensors on satellites, offers global coverage through combined observations, (Hsu, K., et al., 1997) (Meisner and Arkin, 1987) (Scofield, 1987) (Kummerow et al., 1998, 2000) (Simpson et al., 1988) (Hou et al., 2014).

The 1997-developed PERSIANN algorithm uses sparsely sampled (LEO) and (GEO) satellite data to detect and classify rainfall patterns, utilizing longwave infrared retrievals and daytime visible imagery, with passive microwave imagery continuously adjusting the model's parameters. The algorithm is based on a multilayer neural feedforward network called the Modified Counter Propagation Network and consists of two processes: transformation of infrared images into a self-organizing feature map and mapping of discrete SOFM clusters to outputs (Sorooshian et al. 2000, 2002). PERSIANN-CCS is a cloud-patch-based algorithm that extracts features from infrared cloud images under specific temperature thresholds. It involves four steps: segmentation using an incremental temperature threshold (ITT), extraction of features like temperature, geometry, and texture, classification using self-organizing feature map (SOFM) clustering algorithm, and developing a relationship between brightness temperature and rainfall rate. A PMW rainfall calibrated PERSIANN-CCS algorithm was developed in 2014 and is part of the NASA GPM IMERG algorithm. The data is available for public use through the CHRS Data Portal (Hong et al. 2004) (Karbalaee et al. 2017).

Study Area:

Wadi Araba Basin is located on the coast of the Gulf of Suez, where it ends in the Suez Gulf at the city of Az-Za'faranah, which is one of the coastal cities on the Suez Gulf belonging to the Red Sea Governorate. The basin is bordered to the north by the basins of Abu al-jirayfat and Ghweibba basins, while it is bordered by Wadi Sannur to the northwest, west, and southwest, while it is bordered to the south by the basins of Al-Tarfah, ad-Dahal, El-Deir, Al-Jarf, and Thelemet, and to the east by the Suez Gulf. the study area extends between latitudes 28˚ 32′ 9.7″ - 29˚ 15′ 48.5″ north and longitudes 31˚ 45′ 25.4″ - 32˚ 39′ 47.9″ east, (Fig. 1). the study area is about 4301.2 km2, with 37 sub-basins ranging in area from 10.2 to 1382.3 km2, which extends from the southwest to the northeast with a general slope with a length of 97 km, so that the basin represents a dividing area between the Jabal al-Jalalah al-Bahariyyah Plateau in the north and the Jabal al-Jalalah al-Qibliyyah Plateau in the South. Two mains cross roads extend within the basin: the first is the Al-Kuraymat Az-Za'faranah Road, with a length of 94.3 km, and the second is the Beni Suef Az-Za'faranah Road, with a length of 91.6 km. The Suez-Hurghada Road also passes through the lower part of the valley, with a length of 19.1 km.

DEM:

By using the topographic maps with scales of 1: 50.000 and 1: 25.000, digital elevation models (DEM) downloaded from (USGS), and satellite images of Landsat 8 (OLI), the general elevation condition of the study area shows that the elevations ranged between sea level in the east where the coastal plain was appeared and 1487m in the high crests south east of the basin and in northern Slopes of al-Jalalah al-Qibliyyah Plateau, (Table 1) and (Fig. 2). The basin appeared as a separated area between the Jabal al-Jalalah al-Bahariyyah Plateau in the north and the Jabal al-Jalalah al-Qibliyyah Plateau in the South, so the basin surface slope graduality from the north to the south in the north, from the south to the north in the south and from west to east in the middle. 197.9 km^2 with 4.6% of the study area was less than 100m level, these areas represent the coastal plain and downstream area, while 1508.2 km^2 with 28.7% of the study area tope than 500m level as the highest parts which appear in the south of the basin and some parts in the north. The elevations between 100 – 200m cover about 9.7% of the study area which is the lower parts of the southern and northern mountain slopes. The elevations of >200m cover about 85.7% of the study area which distributed in the south as the extent of al-Jalalah al-Qibliyyah Plateau.

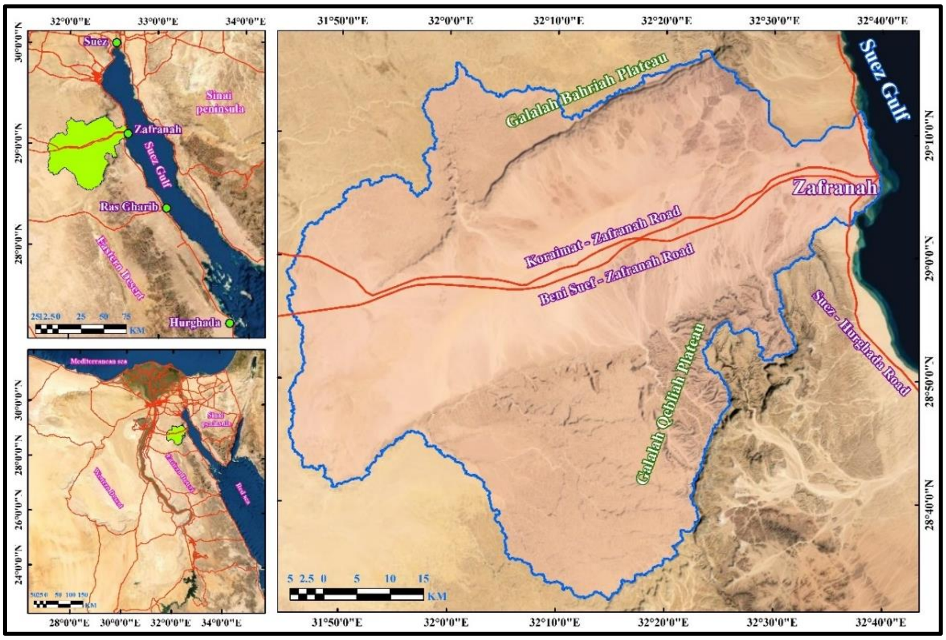

Fig. (1) location map of The Study Area

Slope:

Flat and semi-flat land with slope less than 2° cover about 7.9% of the study area, which located in the coastal plain and downstream area, while gentle land with slopes between 2°-5° cover about 25.9% of the study area which distributed in Pedi plains and wadis bottoms, (Table 1) and (Fig. 2). Moderate and moderately steeps with slopes between (5°-10°) (10°-18°) cover 47% of the study area which distributed in the middle of the basin and along the slopes of south and north elevated areas. Steep and very steep land with slopes between (18°-30°) (30°-45°) cover about 12.3% of the basin's area located in the slopes of Jabal al-Jalalah al-Bahariyyah Plateau in the north and the Jabal al-Jalalah al-Qibliyyah Plateau in the South, while precipitous lands with slopes over than 45° cover 0.3% of the area which appeared in the mountain areas in the north and south.

Table (1) Study area topographical characteristics

	Type	Area (km^2)	(%)
Elevation	-100	197.9	4.6
	-200	417.7	9.7
	-300	1345.6	31.3
	-400	530.1	12.3
	-500	301.7	7
	-1000	1056.7	24.6
	1000+	451.5	10.5
Slope	0 - 2	341.6	7.9
	2 - 5	1113.2	25.9
	5 - 10	1399	32.5
	10 - 18	906.2	21.1
	18 - 30	424.8	9.9
	30 - 45	105.4	2.4
	45 +	11	0.3
Aspect	Flat (-1)	548.3	12.7
	N	437.4	10.2
	NE	387.4	9.0
	E	458.9	10.7
	SE	556.4	12.9
	S	502.8	11.7
	SW	432.2	10.0
	W	454.9	10.6
	NW	522.9	12.2

Aspect:

According to (Fig. 2) and (table 1) 12.7% of study area is flat which located in the coastal plain, downstream area and wadis bottoms, while 31.4% of the study area are oriented to the north where the slopes of Jabal al-Jalalah al-Qibliyyah Plateau are located. The south direction is the most aspects founded in the study area which cover about 34.6% which located in the slopes of Jabal al-Jalalah al-Bahariyyah Plateau in the north. East and south direction cover about (10.7 – 10.6%) respectively which appears in the east and west of the basin.

Hypsometric curve:

Hypsometric curve is known as the cumulative Frequency curve of areas or their percentage. It is a graphic line between the area enclosed between two contour lines or the ratio of what each area occupies to the total area represented on the map. (Fig. 3) show that the study area has entered an advanced stage of erosion, which is the Old Stage, where the value of the hypsometric integration reached about 0.35, which means that 65% of the total study area has been carved by erosion factors, and only 35% remained, which explains the prevalence of gentle slopes, the flatness of a large part of the surface, the widening of the plains area, and the dominance of braided canals in the lower parts of the basin and above the alluvial fan.

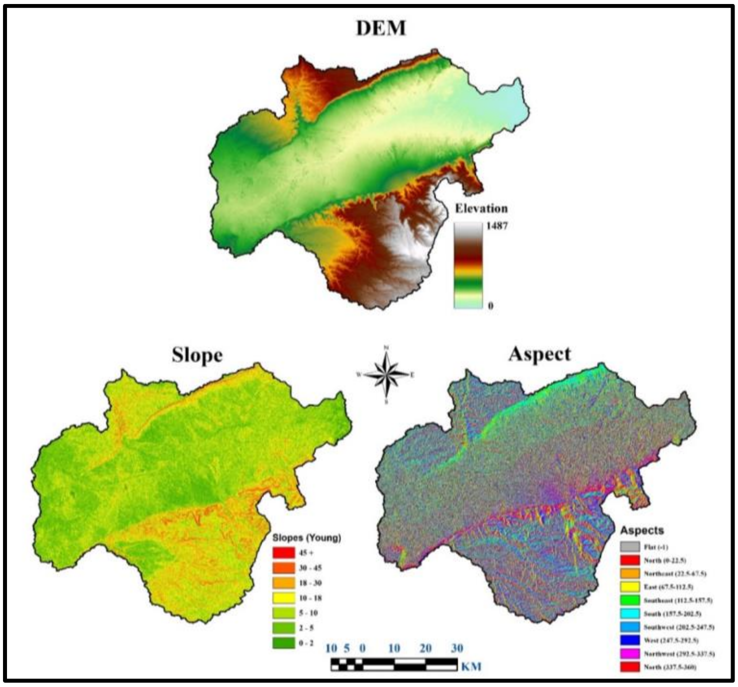

Fig. (2) DEM, Slope, and Aspects of The Study Area

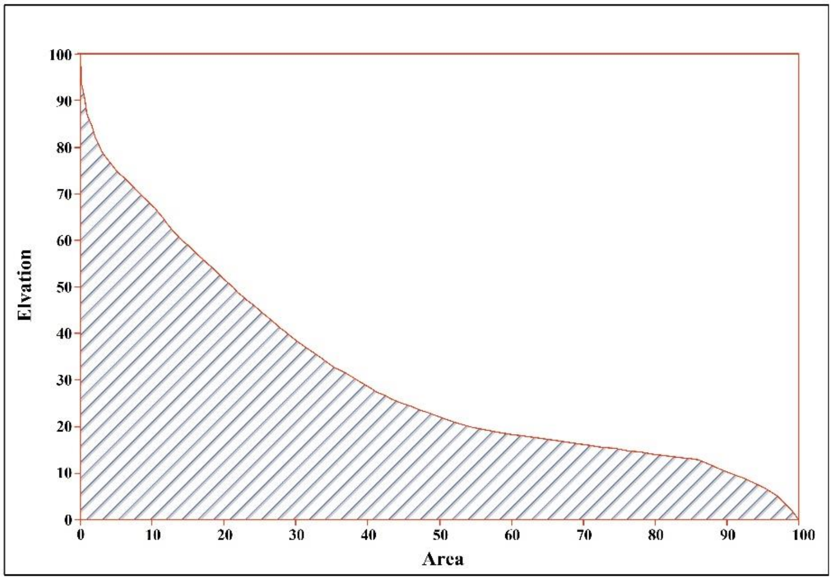

Fig. (3) The Study Area's hypsometric curve

Methodology:

This study depended on three data sources: PERSIANN data, topographic data, and rainfall data, (Fig. 4). PERSIANN data includes four patterns: PERSIANN-CCS, PERSIANN-CDR, PDIR-Now, and PERSIANN-CCS-CDR. This study used the PERSIANN-CCS (Cloud Classification System) pattern, which is a satellite precipitation product developed by the Center for Hydrometeorology and Remote Sensing (CHRS). The CHRS at UCI developed a satellite precipitation product that categorizes cloud-patch features based on height, areal extent, and texture variability, assigning rainfall values to pixels. The topographic data represented on digital elevation model (DEM) which used to extract watershed basins and then estimate wadies morphometry and surface analysis. Rainfall data from climatic station used in calculate water budget and storm return period. Finally, the three data source are used to model the Wadi Flash Floods.

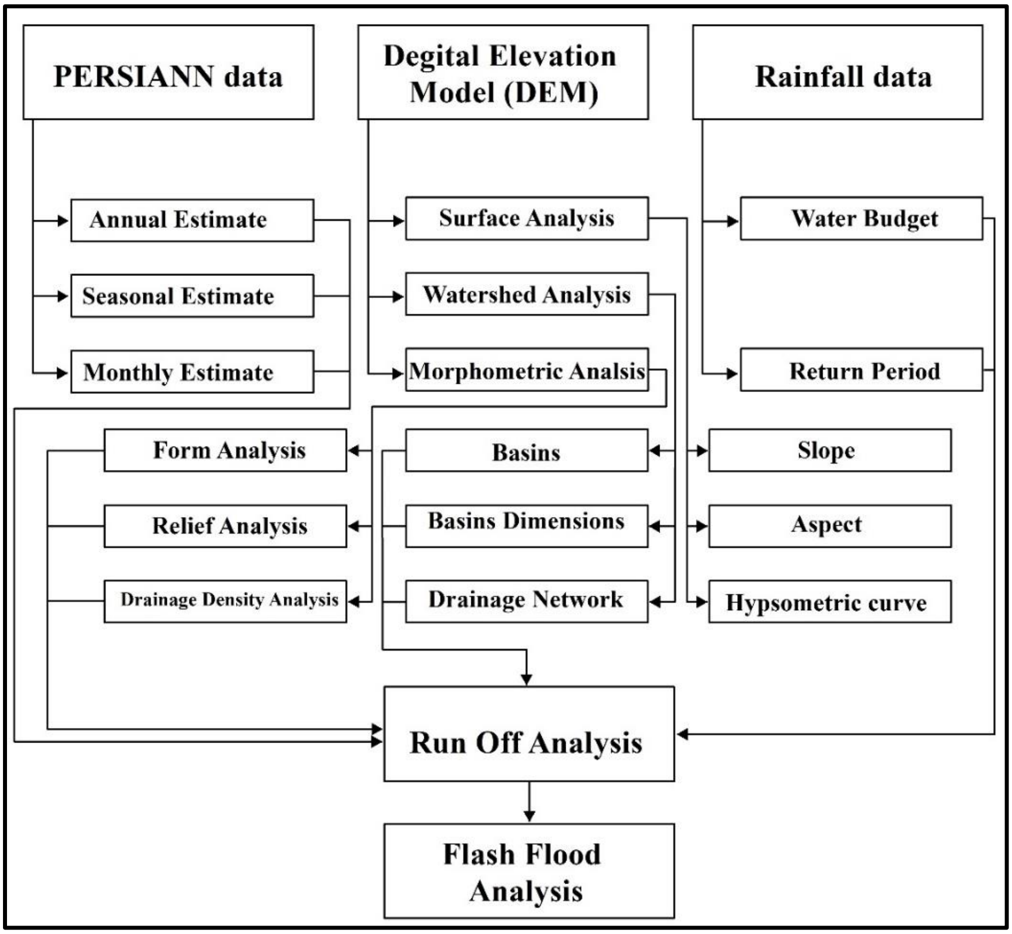

Fig. (4) proposed methodology of the study

Results and discussion:

1. Rainfall estimates from satellite imagery

1.1. Annual precipitation average

the annual precipitation average reached about 9.72 mm per year and therefore Wadi Araba was expected to contain about 41.8 million m³ annually at least, as this value increased during some years that have high precipitation ratio as well as during some months with higher ratios of rain storms in both quantity and quality. (Table 2) (Fig. 5) and (Fig. 6) show annual variation in precipitation volume in the study area which indicates that the year 2018 has the highest potential precipitation volume among all other years of the study with an annual average reached about 19.85 mm which consequently loads Wadi Araba with about a volume of water reached about 85.4 million m³. This volume increased during some months and disappears during others. the fluctuation in rainfall volume expected to fall on Wadi Araba basin along the study period (2015 – 2021), as the general curve for precipitation raised obviously during (2015 – 2018) explaining that the area recorded a huge amount of rain, as many rain storms passed through the area most relevant of which was the rain storm on (26^{th} – 27^{th} October, 2016) which provoked many runoffs in whole Egypt leaving many casualties reaching about 26 deaths and 72 injuries, most of these cases were in Red Sea governorates, South Sinai and Suhag. In addition to the storm on (25th – 26^{th} April, 2018) which resulted in breakthrough the Khatamia - Al-'Ain al-Sokhna Road, Al-'Ain al-Sokhna – Az-Za'faranah road, and Al-Kuraymat - Az-Za'faranah road as a result of overwhelming runoffs in the region.

Table (2) Annual average and Seasonal values for potential precipitation for Wadi Araba during (2015 – 2021)

	Year	2015	2016	2017	2018	2019	2020	2021	Ave.
Average	Year Ave.	6.17	10.59	9.86	19.85	11.22	3.83	6.5	9.72
	Total Rain	74	127.07	118.3	238.14	134.67	45.94	78	116.59
	Change (%)	-	71.6	-6.9	101.3	-43.5	-65.9	69.7	21.1
Seasonal	Winter	17.41	3.19	9.71	34.22	23.63	8.62	7.46	14.89
	Spring	4.84	24.28	16.58	41.52	15.93	9.75	7.61	17.22
	Summer	0.68	0.26	0	0.06	0.97	0.19	0.08	0.32
	Autumn	3.45	11.67	1.78	14.21	1.68	1.84	3.05	5.38

Resource: PERSIANN – CCS data analysis during (2015 – 2021).

water volume decreased during the period (2018 – 2020) and thence turns to rise upward gradually during the year 2020 when the general average of potential precipitation reached 6.5 mm due to many rain storms crossing the area during that year, most famous of which was The Dragon Storm on (11, 12,13th March, 2020) causing a dangerous runoff in the northern part of the Eastern Desert where the study area locates. As well as the rainstorm on (2nd November, 2020). Generally, the percentage of change in potential precipitation average for the study area reached 21.1 % which is returned to increase of ratios of strong rainstorms crossing the area in general, a fact that is returned to obvious changes in both number and strength of which increased to a great extent during autumn and spring every year. (Fig. 5) shows spatial changes in potential precipitation volume falling on Wadi Araba basin. It shows that the most majority of precipitation is concentrated on northern and southern parts of the basin area which resembles the southern foots of Jabal al-Jalalah al-Bahariyyah Plateau and the northern foots of Jabal al-Jalalah al-Qibliyyah Plateau which acts as the most important trap for rainstorms crossing the western part of Suez Gulf.

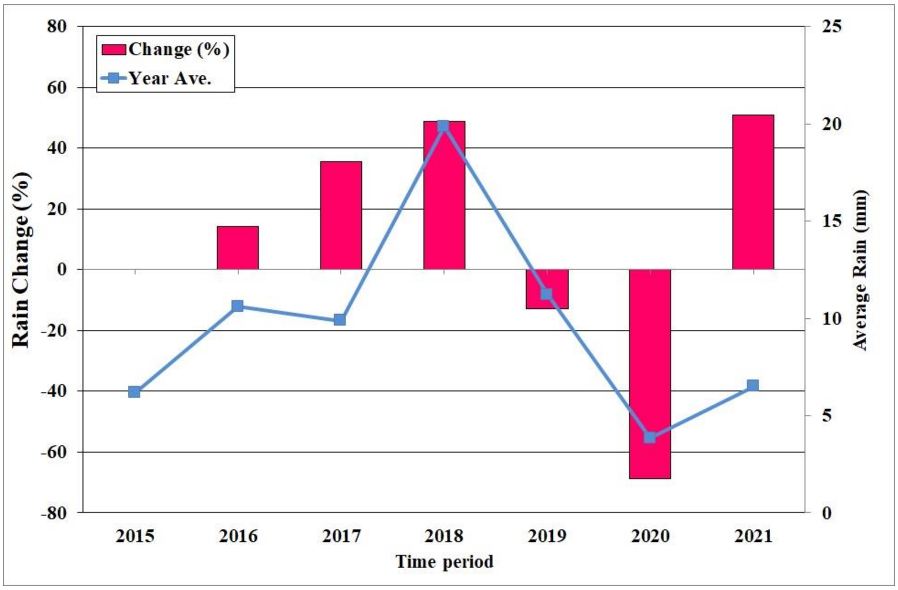

Fig. (5) Annual averages and changes of potential precipitation volume in Wadi Araba basin during (2015 – 2021)

1.2. Seasonal precipitation average in the study area:

potential seasonal averages of precipitation in Wadi Araba illustrated that spring have the highest potential precipitation volume among all other Seasons with an average of about 17.22 mm during the study period which noticeably increased to reach 41.52 mm on spring, 2018 which was related to the increase of rainstorms crossing the area and also to the prevailing weather fluctuations during that year, (Fig. 7). It reached also 24.28 mm on spring 2016. Potential precipitation volume increase was returned to the prominent air disturbances active during this season represented in cyclones crossing the northern parts of Egypt in addition to Khamsin seasonal wind and the consequent increased chances for rainfall. winter comes in the second rank with an average of about 14.89 mm during the study period, as winter is the coldest of all seasons when frequent cyclones cross along the Egyptian northern coasts extending in effect to reach internal parts of northern the Eastern Desert and Red Sea Mountain resulting, thus, in the increase of potential precipitation ratio in Wadi Araba basin. Potential precipitation

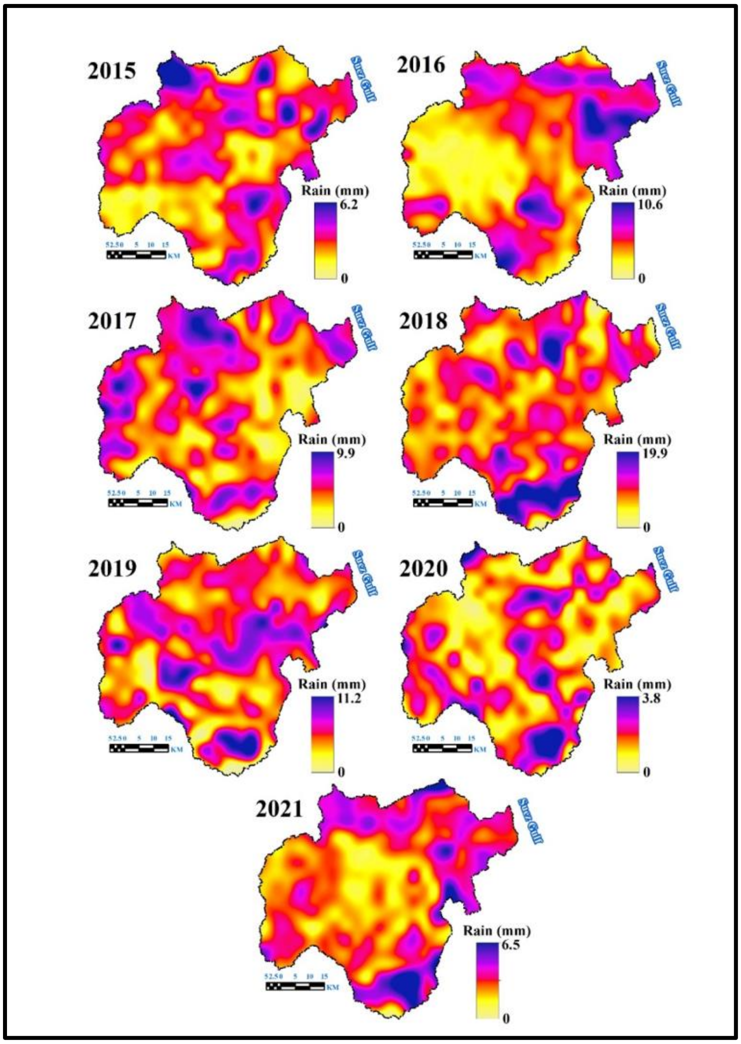

Fig. (6) Spatial and time changes in potential precipitation volume in Wadi Araba basin during (2015 – 2021)

volume in Wadi Araba basin during winter reached its maximum value in 2018 with 34.22 mm followed by winter, 2019 when it reached about 23.63 mm. Whereas the minimum value occurred in the year 2016, as it reached about 3.19 mm which is returned to the crossing cyclones and to the extent it reached within the Egyptian lands. Autumn comes in the third rank of potential precipitation volume with an average of 5.38 mm, which is a transitional period between the dry summer season and the rainfall winter season. Thus, this season has some meteorological fluctuations causing rainfall on the study area. It is considerable to mention that one of the most hazardous floods that Suez Gulf area ever encountered was on autumn, 2016, specifically on 26th – 27th October, 2016. Potential precipitation volume reached its maximum value in autumn in the year 2018 with 14.21, followed by the year 2016 with 11.67 mm. during these years' rainstorm strength increased generally both in quantity and quality leading to many flash floods that the Suez Gulf area witnessed. Summer is the least rainfall season with an average that recorded to 0.32 mm during the study period, as the study area is characterized with its extremely high temperature, dry weather and high moisture during summer.

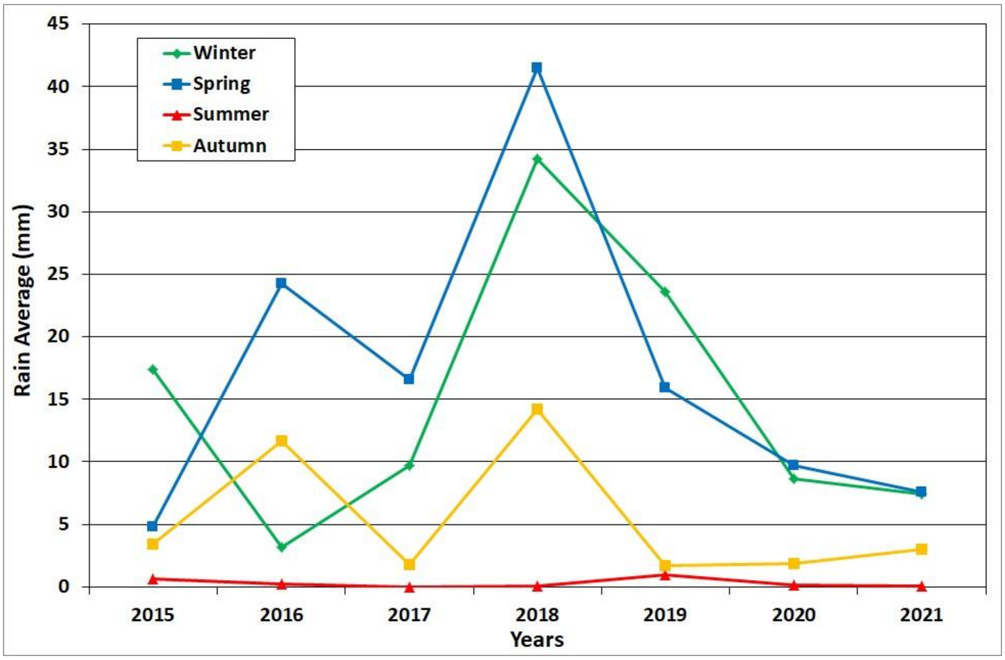

Fig. (7) Change in potential precipitation volume during seasons in Wadi Araba basin during (2015 – 2021)

1.3. Monthly precipitation average in the study area:

potential monthly average for precipitation illustrates that March is the highest among all months of potential precipitation ratio with an average of 19.19 mm during the study period as this month resembles the end of winter and the beginning of spring, thus coincides with the beginning of spring weather fluctuations and its coincident blow of southern warm winds so as to fill cyclones crossing northern coasts and pulled by Red Sea Mountains southwards. Large volume of rain was recorded on March during the years 2016 when potential precipitation volume recorded 45.6 mm, and the year 2018 when final precipitation volume recorded 33.34 mm. whereas December comes in the second rank month of high potential precipitation ratio as it resembles the end of autumn and the beginning of winter and, therefore, temperature tends to decrease. Thus, chances of rainfall increase with the increase of ratio of cyclones crossing the northern coasts especially when some cyclones change its direction southwards through Red Sea Mountains raising, thus, rainfall probability on Wadi Araba basin. Monthly precipitation ratio in December reached 17.68 mm as this month witnessed high potential precipitation ratio reached 44.5 mm during the year 2017, and about 28.74 mm during the year 2021. May and April have the third and fourth rank with a potential precipitation average of about 16.45 mm respectively. The least among all months of precipitation ratio were July, August and June which resemble the months of summer which is a high temperature, prevailing drought conditions and absence of rainfall chances to a great extent except for some convectional rainfall resulting from high temperature with the presence of a source of evaporation represented in Suez Gulf. Such rains are greatly scarce, little in amount and ineffective to the runoff process, (Fig. 8).

1.4. Monthly average of maximum precipitation volume during the study period:

May is the highest of all months recording the highest precipitation volume during the study period. This is returned to the overwhelming floods this month in 2018 leading to breakthrough in all roads leading to Suez Gulf and traffic stop for more than one day because of the rainstorm blew on 25th May, 2018. Maximum precipitation volume recorded during this month was 122 mm on the south-western slopes of Jabal al-Jalalah al-Bahariyyah Plateau, (Table 3). As noticed from the table, the monthly average of maximum precipitation volume decreased gradually with the approach of months of spring, winter and autumn and disappeared in some summer months. Averages of precipitation volume recorded during April, March and February reached (57.43 – 53.46 – 52.0 mm) respectively. Therefore, it is noticeable that spring is the highest season concerning maximum precipitation volume recorded with an average of about 57.71 mm during March – April – May) in comparison to 49.9 mm during winter, 27.0 mm during autumn and 7.24 mm during summer. Winter is also increase in precipitation ratio, as February recorded the highest ratio for maximum precipitation volume reaching about 52.0 mm, followed by December reaching about 51.0 mm, these months have many crosses of rainstorms probable to cause large precipitation volume. During autumn the area begins to receive rainstorms and therefore the area receives reasonable precipitation volume. November is the highest month recorded about 42.29 mm. this amount raised to reach 67 mm in 2018, 56 mm in 2016, and 54 mm in 2019. Whereas summer months are low potential precipitation ratio with an average of about 7.24 mm; as precipitation ceases during some months due to high temperature, severe draught, disappearance of crossing cyclones in the north and extending extremities of low pressure from Sudan in the south and India in the east towards the Egyptian lands and therefore alleviates chances of precipitation.

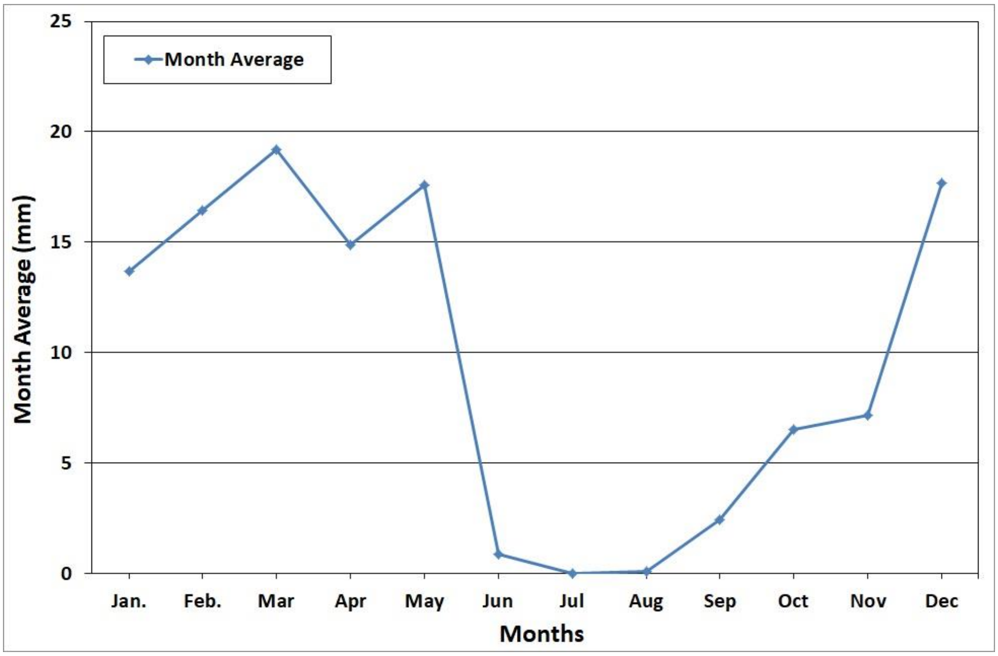

Fig. (8) Change in potential precipitation volume for all months in Wadi Araba basin during (2015 -2021)

Table (3) Monthly average of maximum, minimum, and average precipitation volume recorded in Wadi Araba during (2015 – 2021)

Months		Jan.	Feb.	Mar	Apr	May	Jun	Jul	Aug	Sep	Oct	Nov	Dec	Year Average
2015	Max.	62.0	53.0	37.0	25.0	20.0	18.0	0.0	1.0	7.0	26.0	21.0	20.0	24.2
	Min.	11.0	7.0	1.0	0.0	0.0	0.0	0.0	0.0	0.0	1.0	0.0	0.0	1.7
	Mean.	26.4	19.2	12.7	0.9	0.9	2.0	0.0	0.0	0.4	6.7	3.2	1.5	6.2
2016	Max.	2.0	28.0	84.0	34.0	49.0	19.0	0.0	26.0	0.0	26.0	56.0	33.0	29.8
	Min.	0.0	0.0	32.0	1.0	4.0	0.0	0.0	0.0	0.0	6.0	5.0	2.0	4.2
	Mean.	1.0	7.0	45.6	9.0	18.2	0.6	0.0	0.2	0.0	14.3	20.7	10.4	10.6
2017	Max.	63.0	5.0	50.0	68.0	44.0	0.0	0.0	0.0	0.0	10.0	32.0	89.0	30.1
	Min.	3.0	0.0	1.0	8.0	2.0	0.0	0.0	0.0	0.0	0.0	0.0	13.0	2.3
	Mean.	18.6	0.1	12.1	23.8	13.9	0.0	0.0	0.0	0.0	0.1	5.2	44.5	9.9
2018	Max.	15.0	145.0	91.0	75.0	122.0	0.0	0.0	12.0	74.0	51.0	67.0	55.0	58.9
	Min.	0.0	17.0	11.0	2.0	34.0	0.0	0.0	0.0	3.0	4.0	1.0	1.0	6.1
	Mean.	0.6	57.6	33.3	24.9	66.3	0.0	0.0	0.2	16.6	16.2	9.8	12.6	19.9
2019	Max.	109.0	71.0	36.0	78.0	68.0	38.0	0.0	0.0	0.0	6.0	54.0	46.0	42.2
	Min.	0.0	3.0	1.0	12.0	0.0	0.0	0.0	0.0	0.0	0.0	0.0	1.0	1.4
	Mean.	38.1	20.2	11.0	29.8	7.0	2.9	0.0	0.0	0.0	0.4	4.6	20.6	11.2
2020	Max.	47.0	13.0	56.0	23.0	43.0	8.0	0.0	17.0	19.0	13.0	37.0	26.0	25.2
	Min.	0.0	0.0	3.0	0.0	0.0	0.0	0.0	0.0	0.0	0.0	0.0	1.0	0.3
	Mean.	4.0	1.2	18.9	2.1	8.3	0.3	0.0	0.3	0.2	0.2	5.1	5.4	3.8
2021	Max.	29.0	49.0	20.0	99.0	90.0	13.0	0.0	0.0	0.0	39.0	29.0	88.0	38.0
	Min.	1.0	1.0	0.0	1.0	0.0	0.0	0.0	0.0	0.0	0.0	0.0	5.0	0.7
	Mean.	7.3	9.7	0.7	13.5	8.6	0.2	0.0	0.0	0.0	7.7	1.5	28.7	6.5
Month Average	Max.	46.7	52.0	53.4	57.4	62.3	13.7	0.0	8.0	14.3	24.4	42.3	51.0	35.5
	Min.	2.1	4.0	7.0	3.4	5.7	0.0	0.0	0.0	0.4	1.6	0.9	3.3	2.4
	Mean.	13.7	16.5	19.2	14.9	17.6	0.9	0.0	0.1	2.5	6.5	7.2	17.7	9.7

1.5. Monthly average of minimum precipitation volume during the study period:

March has the highest potential precipitation ratio with an average of 7.0 mm during the study period, this is due to the rainfall on March 13th 2016, as satellite imagery shew large number of clouds with a probability of heavy rain reached 32 mm as a minimum amount in the study area during this month, (Table 3). May comes in the second rank with an average of about 5.71 mm during the study period, as it recorded high precipitation ratio during the year 2018, as it reached about 34 mm during this month. February comes in the third rank of minimum precipitation volume recorded with an average of 4.0 mm during this month. February recorded potential precipitation volume reached about 17 mm in the year 2018. Regarding seasons, spring recorded the highest ratio for minimum precipitation volume recorded according to satellite imagery analysis with an average of 5.38 mm, followed by winter with an average of 3.14 mm, then autumn with an average of about 0.95 mm. Whereas summer did not record any potential precipitation volume as a minimum precipitation volume during the study period.

1.6. Annual analysis of potential precipitation volume averages during the study period:

(Table 3) and (Fig. 9) and (Fig. 10) shows annual precipitation averages recorded during the study period (2015 -2021), which show the following:

2015: Annual precipitation averages reached 6.17 mm. This average raised during January to 26.36 and decreased to zero during August and July. Winter is the highest season concerning potential precipitation average which reached 17.41 mm, followed by spring 4.84 mm.

2016: One of the most significant years, which potential precipitation volume average reached 10.59. This value increased to reach 45.58 during March, whereas October had a hazardous runoff in the middle and southern parts of Suez Gulf resulting in submerging most of Ras Gharib city, 100 kilometers southern Az-Za'faranah city. Spring season had the highest value of potential precipitation ratio which reached 24.28 mm, followed by autumn with 11.67 mm, then winter with3.19 mm.

2017: Potential precipitation average lower during this year than the next year as it reached 9.86 mm. This average highest in December which recorded 44.5 mm, followed by April with 23.82 mm. Spring is the first rank with 16.58 mm, followed by winter 9.71, then autumn with 1.78 mm.

2018: This year is the highest among all study years of potential precipitation ratio monitored through satellite imagery as the general average was 19.85 mm, this volume reached its highest value during May with 66.33 mm as it witnessed a strong crossing rainstorm on 25th May, resulting in a great runoff in the Wadis of the northern and middle parts of Suez Gulf. February is the second rank during this year as it reached 57.6 mm. Spring season record the highest precipitation ratio with an average of about 41.52 mm, followed by winter with about 34.22 mm, then autumn with 14.21 mm.

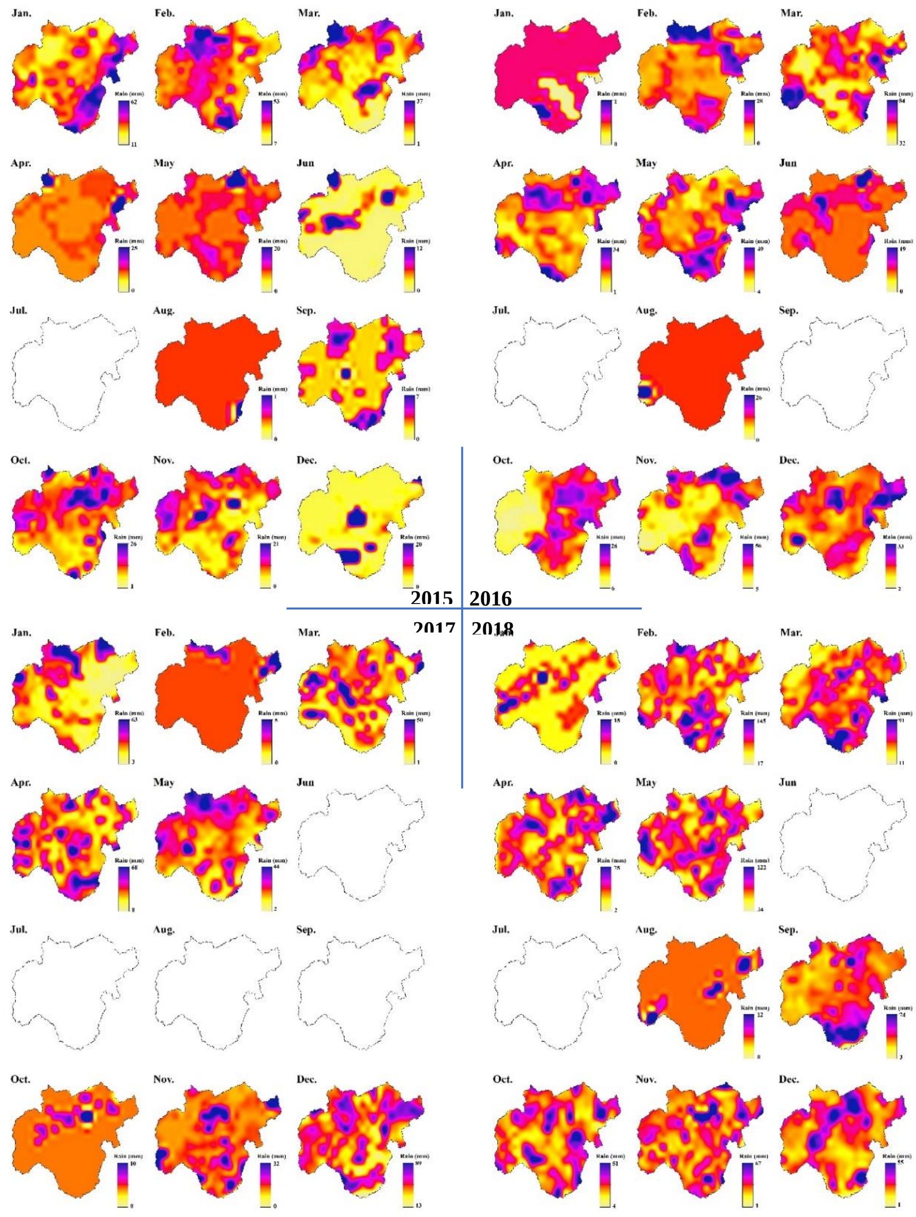

Fig. (9) Expected monthly precipitation in Wadi Araba basin during (2015 – 2018)

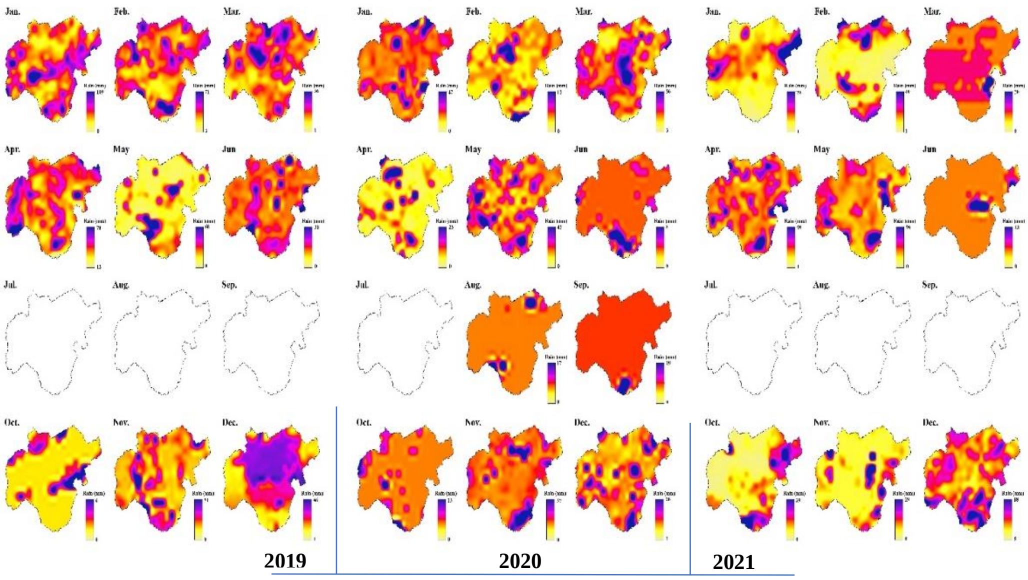

Fig. (10) Expected monthly precipitation in Wadi Araba basin during (2019 – 2021)

2019: Annual precipitation average decreased during this year than the previous one; which reached 11.22 mm, with a decline rate of 43.5 %. January is the highest month which reached about 38.05 mm, followed by April reached 29.78 mm. winter is the highest season which reached 23.63 mm, followed by spring of about 15.93 mm, then autumn with 1.68 mm.

2020: average of potential precipitation during this year was 3.83 mm, thus it is the least of all study years of potential precipitation ratio due to lack in crossing cyclones and therefore reduction in its impacts. One reason for this is the reduction of human activities because of corona virus spread, affecting thus some weather conditions. March is the highest month with an average of about 18.9 mm, as this month was affected by the crossing of the Dragon storm extending for three days – (11th – 12th- 13th of March) – leading to subsequent floods in the northern part of the Eastern Desert within which the study area is located.

2021: During this year the general average of precipitation increased to reach 6.5 mm with an increase rate of 69.7 % than the previous year. December is the highest month considering precipitation ratio with 28.74 mm, followed by April with 13.54 mm. Whereas Spring and winter are the highest seasons of precipitation ratio which reached 7.61, 7.47 respectively.

2. Wadi Sub-Basin Morphometry

Wadi Araba Basin includes 37 sub-basins, (Table 4) and (Fig. 11), whose characteristics vary as follows:

2.1. Basin Scale Parameter

The study area's basins are small, with areas ranging from 10.2-1382.3 km2, lengths from 6.2-69.2, widths from 1.3-16.7 km, and perimeters from 15.9-309.5 km. These basins are prone to rainstorms and decrease of losses through seepage and evaporation. Short-length basins are the most dangerous, as surface runoff water can reach valley exits quickly. They also have a large surplus of water due to less loss through evaporation and leakage compared to longer valleys. These basins are characterized by danger, as they can be covered and affected by rainstorms.

2.2. Basin Shape Parameter

The region's basins are rectangular in shape, with a Circularity ratio with average of 0.36 and an Elongation ratio with average of 0.49, indicating low flood risk. The Form factor is triangular, reducing the risk of torrent flow, which average is 0.20. High Lemniscates values which ranged from (0.38-3.47) indicate less flattened basins with low-risk rates. High Compactness values which ranged from (1.12-2.46) indicate irregularity. The consistency of most valleys and high meander of perimeters indicates an early stage of erosional cycles, resulting in high-risk rates. The high Length/Width values ranged from (1.38-10.92) indicate some basins are in a young stage, as most elongate. Current climatic and geological conditions may continue this stage for a period. The high Length/Width values suggest that the basins are in a young stage, with most elongating basins.

2.3. Basin Topography Parameter

The basins in the region have higher relief values (m) compared to some of the Red Sea mountains sloping towards the Nile River due to their small area and lack of extension in the mountain range. The relief ratio or Mean basin slope ranges between (8.66-69.74) with an average of 36.6, reflecting the short lengths of the basins and high relief rates. The relative relief ranges between (0.35-2.53) with an average of 1.45, reflecting the intensity of rocks' resistance to erosion factors. The roughness number ranges between (0.13-6.86) with an average of 3.02, reflecting the stage of erosion through which the basins pass. The Hypsometric Integral values (0.03-1.09) indicate the study area was affected by various erosion factors, while the slope ratio (0.38-1.79) indicates low rates of surface slope due to its location in the valley's belly.

Table (4) Morphometry of the study area Basins

Parameter	Unit	Range	SD	Formula	Reference
Area (A)	(km2)	10.2-1382.3	223.3	*Basin Area*	*Schumm, 1956*
Basin length (Lb)	(Km)	6.2-69.2	12.1	*Maximum Basin length*	*Schumm, 1956*
Basin Width (W)	(Km)	1.3-16.7	3.3	*Mean Basin Width*	*Schumm, 1956*
Perimeter (Pr)	(Km)	15.9-309.5	48.8	*Basin Perimeter*	*Schumm, 1956*
Elongation ratio (Re)	-	0.3-0.91	0.14	$R_e = 2A/\pi/L_b$	*Schumm, 1956*
Circularity ratio (Rc)	-	0.17-0.79	0.15	$R_c = 4\pi A/P_r^2$	*Miller, 1953*
Form factor (F)	-	0.07-0.66	0.12	$F = A/L_b^2$	*Horton, 1932*
Compactness (C)	-	1.12-2.46	0.33	$C = P_r/2\sqrt{\pi A}$	*Horton, 1932*
Lemniscates (K)	-	0.38-3.47	0.80	$k = L_b^2/4 \times A$	*Gregory & Walling, 1973*
Length / Width (LW)	-	1.38-10.92	2.30	$LW = L_b/W$	*Muller,1974*
Relief (R)	(m)	56-1402	408.6	$R = (H_{max} - H_{min})$	*Strahler, 1952*
Relief ratio (Rr)	-	8.66-69.74	17.69	$R_r = R/L_b$	*Schumm, 1956*
Relative relief (Rf)	-	0.35-2.53	0.71	$Rf = R/P_r \times 100$	*Schumm, 1956*
Ruggedness number (Rn)	-	0.13-6.86	1.67	$R_n = R \times D_d$	*Melton, 1958*
Mean basin slope (Sb)	(m)	33-821.5	17.69	*Average basin slope*	*Zhou et al., 2016*
Mainstream slope (Sms)	%	7.67-54.85	15.19	$S_{ms} = R/ms$	*Al-Rawas, 2010*
Slope ratio (Rs)	-	0.38-1.79	0.19	$R_s = S_{ms}/S_b$	*Al-Rawas, 2010*
Hypsometric Integral (HI)	-	0.03-1.09	0.19	$HI = A / R$	*Pike, & Wilson, 1971*
Stream order (Su)	-	4-7	0.69	*Hierarchical rank*	*Strahler, 1957*
Total stream number (TNs)	-	27-3380	544.9	*Total stream number*	*Horton, 1945*
Total streams length (TLs)	(Km)	23.8-3333.9	524.4	*Total streams length*	*Horton, 1945*
Bifurcation ratio (Rb)	-	2.6-5.9	0.63	$R_b = Nu/Nu+1$	*Horton, 1932*
Drainage density (Dd)	(km-1)	2.15-12.04	2.21	$D_d = TL_S/A$	*Horton, 1932*
Drainage frequency (Df)	(km-2)	2.1-2.96	0.21	$D_f = TN_S/A$	*Horton, 1945*
Channel maintenance (Cm)	(Km)	0.08-0.47	0.12	$Cm = 1/D_d$	*Schumm, 1956*
Overland flow length (Lo)	(Km)	1.07-6.02	1.11	$Lo = 1/2D_d$	*Horton, 1945*
Texture ratio (Rt)	(km-1)	1.36-10.92	2.04	$Rt = TN_S/P_r$	*Smith, 1950*

ms = Mainstream length, SD = Stander Deviation

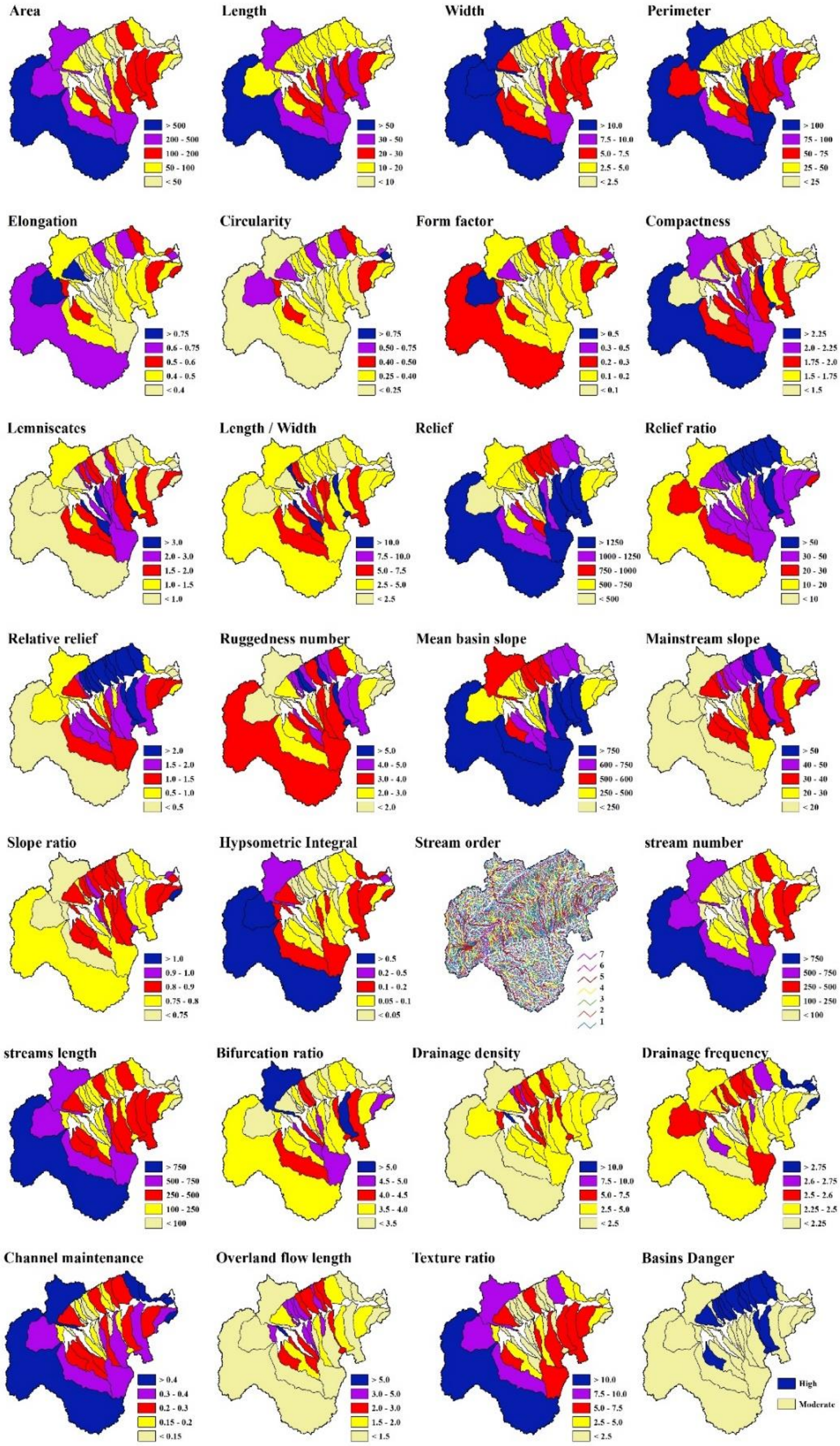

Fig. (11) Wadi Araba Sub-Basins Morphometric Parameters

2.4. Basin Drainage Network Parameter:

The Wadi Araba basin's water drainage networks are large, ranging from fourth to seventh rank, with stream numbers ranging from 27 to 3380, stream lengths from 23.8 to 339.2 km, and bifurcation ratios from 2.6 to 5.9. These networks pose a risk due to the short waterways causing less loss and the water reaching the basin's outlet quickly in many basins.

2.5. Basin Drainage Density Parameter:

The basins in the region have low to moderate drainage density, ranging from 2.15-12.04 km/km2, influenced by geological structure, drought, and small area. The topographic texture is rough in 24 basins, medium in 12 basins, and smooth in the Arkes Basin. The stream frequency ranges from 2.1-2.96 km2, indicating fewer streams and reducing flood risk. The stream maintenance ranges from 0.08-0.47 km2, indicating that the basin area expands at the expense of its limited network length, resulting in decreased discharge density. Overland flow rates range from 1.07-6.02 km2, with an average of 2.25, affecting the basins due to the intensity of drainage and the geological conditions. The basins also have a low to moderate overland flow rate, affecting the overall drainage intensity due to the region's geological conditions.

2.6. Basin Parameter correlation:

The study analyzed the relationship between basin characteristics using correlations between morphometric parameter. The coefficient of determination (R2) was classified into five levels: very strong (0.9–1), strong (0.65–0.9), good (0.35–0.65), weak (0.1–0.35) and very weak (0–0.1). A linear intercorrelation matrix was created to highlight dependent and independent morphometric parameters, (Fig. 12). The results provide valuable insights into the hydrologic response of basins. The study found that basin scale parameters are strongly related to stream lengths, topographic texture, and wadi perimeter, while shape and topographic characteristics have weak relationships. Basin shape elements are strongly related to themselves, with moderate relationships with drainage density parameters. topographic characteristics are strongly related to basin slope, main stream length, and ruggedness number, with low and moderate relationships with other elements. drainage network parameters are strongly related to basin scales and topographic texture, while drainage density parameters are strongly related to themselves and the topographic texture.

2.7. Basin Flash Flood Risk Assessment:

The integrated assessment matrix (IAM) method was used to study flood risks in the region due to its comprehensiveness and high accuracy. The method involved 27 parameters to determine the degree of flood risk in the basins. Morphometric factors were studied and classified into categories based on flash flood severity. The third category was considered extreme danger, with 18 factors. However, some factors, such as length, width, perimeter, lemniscates, length/width, hypsometric integration, total streams length, bifurcation ratio, and channel maintenance, represented the first category. This is due to the geomorphological, structural, and hydrological conditions affecting the basins. A single basin may fall into the first category in some factors, and in the second or third category in other factors. The average degree of risk was calculated for each basin in different treatments, and the degree of risk was calculated for all transactions as a whole. It was found that 23 of the region's basins fall into the medium risk category, 14 into the high-risk category, and none fall into the low or very dangerous flow category.

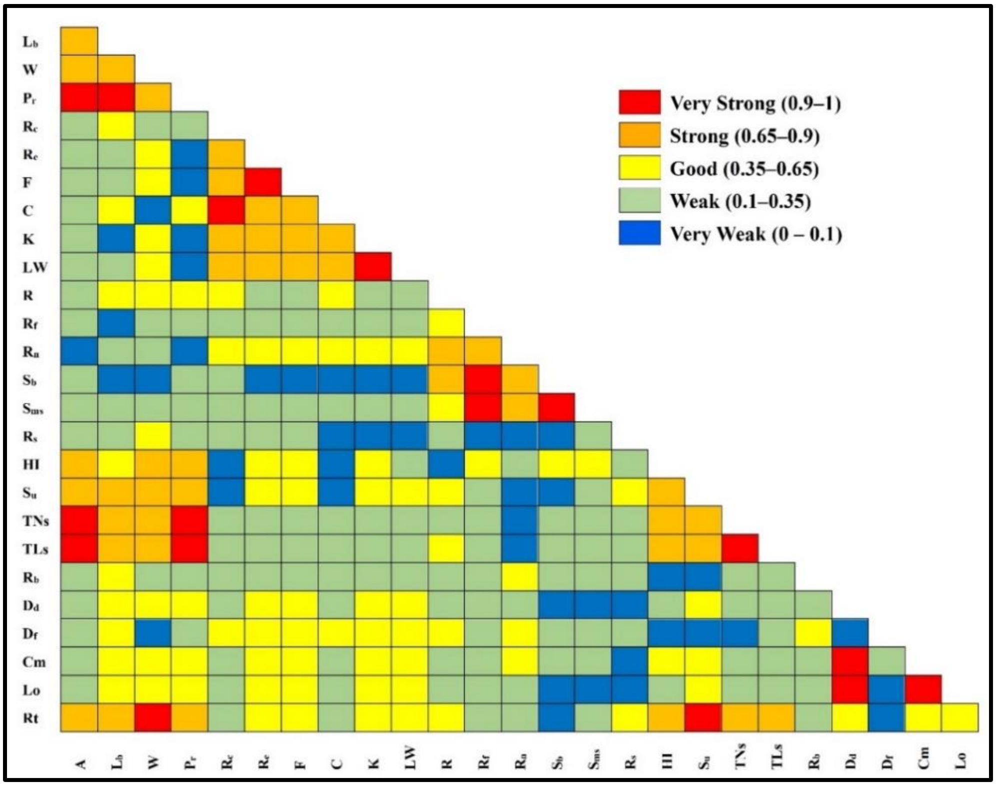

Fig. (12) Correlation matrix between the assessed morphometric parameters

2.8. Basins Hydrological Budget:

The hydrological budget is calculated by calculating water volumes on drainage basins and losses through evaporation and leakage to determine net runoff and Flash Flood runoff. The study area's rainfall ranged from 0.259-35.11 million m3, with the largest rainfall in one day at Suez station reaching 25.4 mm. The average annual evaporation was 8.8 mm, resulting in Evaporation Losses ranging from 0.930-899.78 thousand m3. Lag time infiltration and seepage also varied which ranged between (0.135-1122.41 thousand m3) and (0.401-387.73 thousand m3), respectively, while total losses ranging from 1.612-2409.9 thousand m3. The runoff in the basins ranged from 0.257-32.70 million m3, posing a threat to facilities built in the region. Measures to protect this amount include constructing protection dams on wadi streams or extending drainage channels for water away from installations.

3. Estimating the probability of rainstorms return period:

The study analyzed the probability of flash floods in a specific area using data from meteorological stations. The highest amount of rain fell in one day during 2015-2021, (Rain max (mm), reaching 21 readings, with the highest value being 25.4 mm at Suez station in 2020 and 9.0 mm at Bir Arida station in 2016. The highest rainfall value was ranked first, followed by the rest. The amount of rainfall over the Red Sea Mountains (RRSM) was calculated as an increase of 25% over the same period, (Gheith & Sultan, 2002). The probability of torrent flow in the area (P (%)) was calculated using the equation from Critchley & Siegert (1991).

$$P\ (\%) = (m-0.375)/(N+0.25) \times 100$$

Where ***P*** is probability in % of the observation of the rank m, ***m*** is the rank of the observation, ***N*** is total number of observations used.

The study reveals a 2.9% probability of a Flash Flood on March 12, 2020, the strongest torrent in the region during the study period, due to the inverse relationship between water amount and the probability of occurrence. Large floods are less likely to occur than small ones, and the return period of floods, ***Tp (yr),*** was calculated using the following equation:

$$Tp\ (yr) = 100 / P$$

Where ***Tp (yr)*** is return period of floods and ***P*** is probability in % of the observation of the rank.

the time for the return of floods was calculated, which is inversely proportional to the probability of floods occurring. The probability of a

Flash Flood on March 12, 2020 returning is 35 years. It is predicted that a flood similar in strength to the 2020 flood will occur by 2055, indicating a potential for a similar flood in the future, (Table 5) and (Fig. 13).

Table (5) probability of annual occurrence and return period analysis

Date	year	Rain max (mm)	RRSMG	Rank	P (%)	Tp (yr)
27/1	2016	1.0	1.25	21	97.1	1.03
27/1	2016	1.4	1.75	17	78.2	1.28
27/10	2016	3.4	4.25	8	35.9	2.79
16/2	2017	1.3	1.63	18	82.9	1.21
13/2	2018	1.2	1.5	20	92.4	1.08
25/4	2018	2.3	2.88	10	45.3	2.21
23/11	2018	2.1	2.63	11	50	2
5/12	2018	1.8	2.25	13	59.4	1.68
5/12	2018	1.3	1.63	19	87.6	1.14
6/2	2019	4.6	5.75	6	26.5	3.78
5/3	2019	4	5	7	31.2	3.21
30/3	2019	1.8	2.25	14	64.1	1.56
22/10	2019	3	3.75	9	40.6	2.46
22/10	2019	1.6	2	15	68.8	1.45
24/2	2020	16.4	20.5	2	7.6	13.08
24/2	2020	4.8	6	5	21.8	4.59
12/3	2020	25.4	31.75	1	2.9	34
12/3	2020	9	11.25	3	12.4	8.1
4/2	2021	2	2.5	12	54.7	1.83
5/2	2021	5.2	6.5	4	17.1	5.86
12/11	2021	1.6	2	16	73.5	1.36

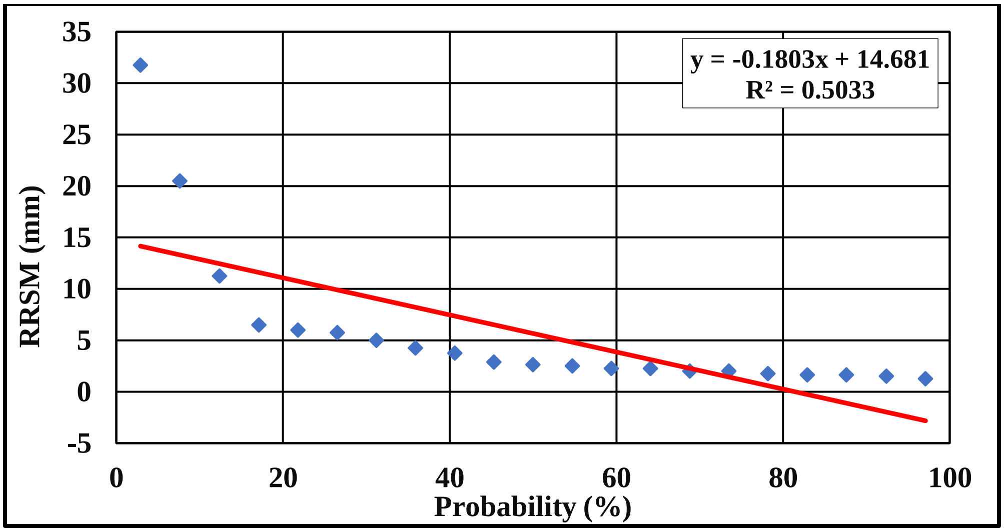

Fig. (13) probability of annual occurrence of the RRSM

4. Modeling Wadi Runoff Based on Satellite Image Data:

Wadi runoff modeling used satellite images data in specific dates to calculate the final wadi runoff by using water budget parameters and assuming that evaporation condition is the same in various rainfall date due to lack of daily evaporation data. Twenty date storm wase selected according to monitor the stormy rainfall during study period. The wadi runoff calculated in both wadi araba and sub-basins. As shown in (Fig. 14) which discuss the estimated wadi runoff in specific rainstorms dates that there was a fluctuation on the amount of wadi araba water volume, where the peak discharge rich about 200 million m^3 in 12 February 2018 and 6 February 2019 due to heavy rain storm attacked the region resulted in a huge wadi flash flood leaving many losses. In the level of sub-basins, the peak discharge ranged between (0.06 – 5.88) million m^3 in 15 February 2015 as a minimum selected rainy storm and between (0.5 – 65.32) million m^3 in 12 March 2018 and 6 February 2019 as a maximum selected rainy storm. The selected rainy storms leaving flash floods greater than 100 million m^3 in 12 times during time period and less than that in 8 times. (Fig. 15) show the selected rainy storms Affected the study area during study time period, which display the hotspots of rain in the selected times. as it clear that the north and south upstream mountain is the heavy concentrated regions of rainy storms if it no cover the whole area of the basin. Also, the rainy storms are various in the total amount of water volume depend on the depth of atmospheric pressure, the extend on the study area, and the period of the storm.

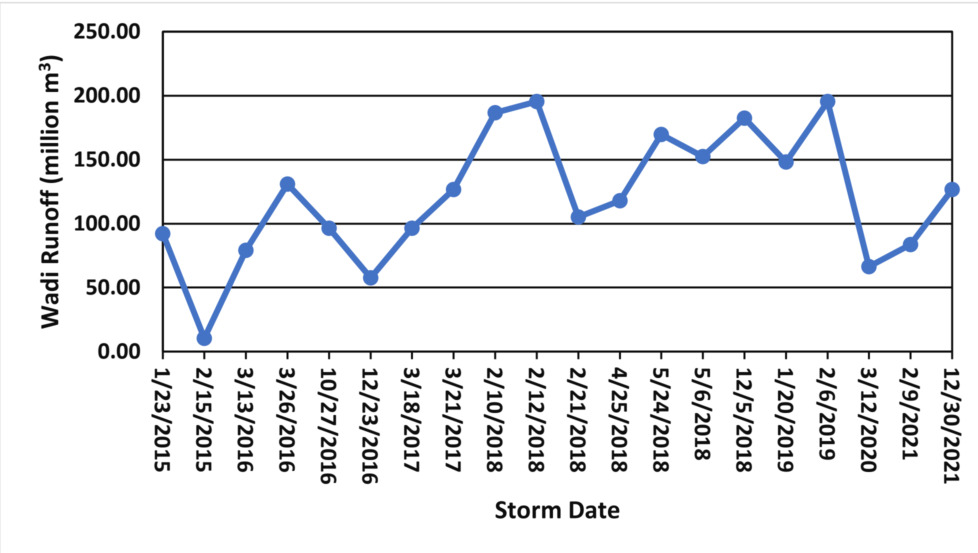

Fig. (14) Estimated Wadi Runoff in specific Rainstorms dates

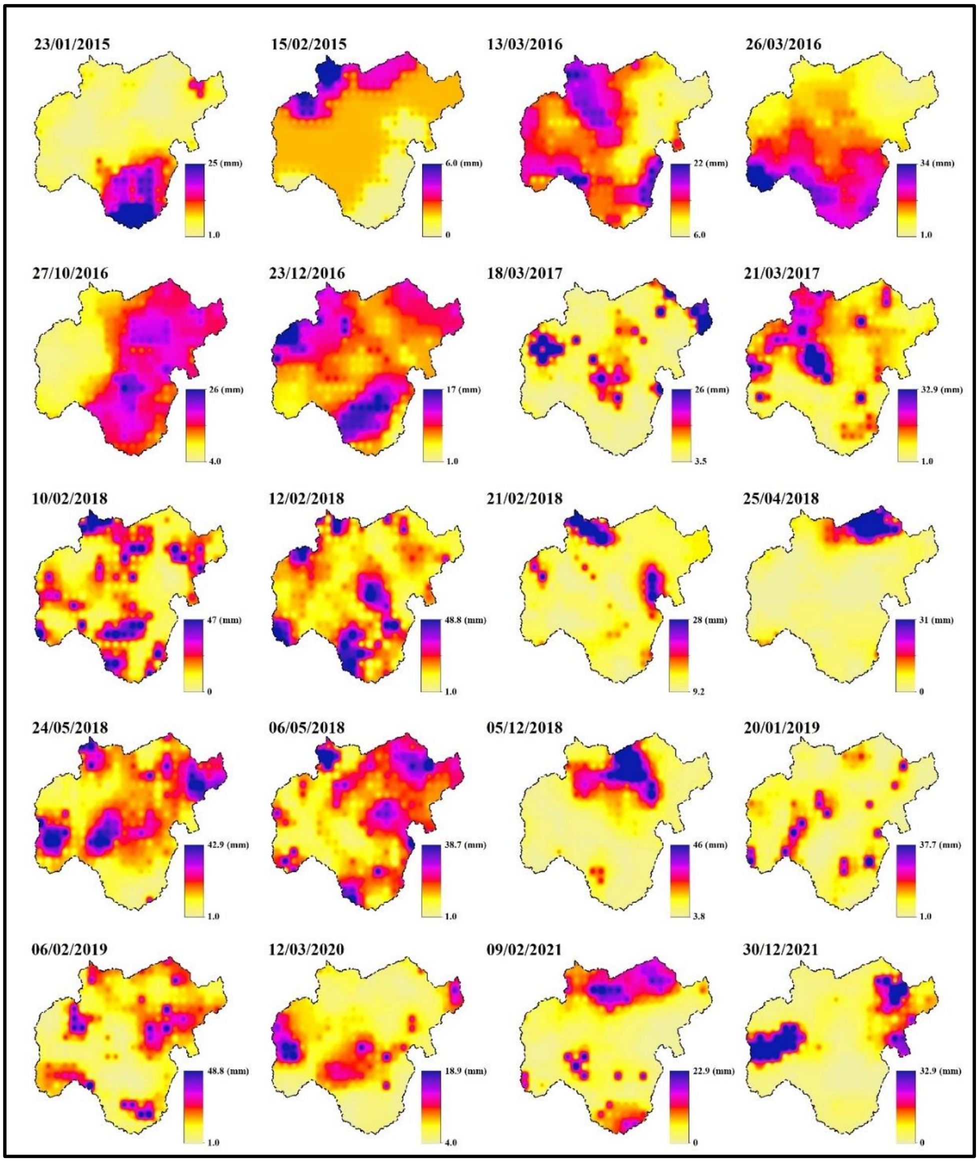

Fig. (15) Selected Rainy Storms Affect Study Area

Conclusion:

This study utilized satellite images and digital data to monitor clouds, calculate precipitation, and estimate flash flood runoff probabilities. The PERSIANN data, represented by the PERSIANN-CCS (Cloud Classification System), was used to estimate the volume of rain expected during rainstorms from 2015-2021 at various levels. The study extracted precipitation values and linked them to flash floods recorded during the study period. A good correlation was found between the precipitation values calculated from PERSIANN-CCS data and data from climatic stations. The study also monitored strong rainstorms and modeled them to calculate flash floods from Wadi Araba and its sub-basins. The topographic data on the digital elevation model (DEM) was used to determine water division areas and extract the Wadi Araba basin and its sub-basins, and calculate water drainage network measurements. This data was then used to calculate the degrees of danger of these basins based on their morphometric characteristics. The study also used data from climatic stations, including Suez Marine and Bir Arida, to extract the largest amount of rain in one day, calculate the size of recorded rain storms, and verify the quality of satellite data. The data aligned with the observed data . The study suggests upgrading dams' design and storage capacity in valleys to absorb floodwaters effectively. It suggests providing storage lakes for dams to absorb excess water, and constructing water drainage channels behind them to drain excess water, avoiding installations in Wadi Araba basin. The modifications aim to ensure dams can handle the largest floodwater amounts.

Reference:

- *Abdel-Fattah, M., Saber, M., Saber, S., Khalil, M., Sumi, T., Sefelnasr, A., (2017): A Hydrological and Geomorphometric Approach to Understanding the Generation of Wadi Flash Floods, Water 2017, 9, 553.*

- *Al-Rawas, G.A.; Valeo, C. (2010): Relationship between wadi drainage characteristics and peak-flood flows in arid northern Oman. Hydrol. Sci. J. 2010, 55, 377–393.*

- *Badawy, M.M., Khidr,M,M., (2011) : A GIS and RS Based Approach for modeling ungauged small-scale catchments in Mersa Alam, Bulletin of the Egyptian geographical society, Tome LXXXIV, Vol. 84.*

- *Crichley, W. and Siegret, K. (1991): Water harvesting. FAO corporation Document Repository, Available at:* *http://www.fao.org/3/U3160E/u3160e05.htm#3.4%20probability%20analysis.*

- *Ebert, E.E.; Janowiak, J.E.; Kidd, C. (2007): Comparison of near-real-time precipitation estimates from satellite observations and numerical models. Bull. Am. Meteorol. Soc. 2007, 88, 47–64.*

- *Elnazer,A,A., Salman, A, S., Asmoay, A,S., (2017) : Flash flood hazard affected Ras Gharib city, Red Sea, Egypt: a proposed flash flood channel, Nat Hazards (2017) 89:1389–1400.*

- *El Shamy, I. Z., (1985): Quantitative Geomorphology and Surface Water Conservation in Wadi Matulla – wadi Abbad Area, Central Eastern Desert, Ann. Geol. Surv. Egypt, Vol. 15, pp. 348 – 358.*

- *Gheith,H. and Sultan,M. (2002): Constrution of hydrologic model for estimating wadi runoff and ground water recharge in the Eastern Desert, Egypt, Journal of Hydrology, 263, PP. 36-55.*

- *Gregory, K.J. and Walling, D.E. (1973): Drainage Basin. Form and Process: A Geomorphological Approach. Edward Arnold, London.*

- *Hong, Y., Gochis, D., Cheng, J.-T., Hsu, K., & Sorooshian, S. (2007): Evaluation of PERSIANN-CCS Rainfall Measurement Using the NAME Event Rain Gauge Network. Journal of Hydrometeorology, 8(3), 469–482.*

- *Hong, Y., Hsu, K., Gao, X., and Sorooshian, S. (2004): Precipitation estimation from remotely sensed information using an artificial neural network – cloud classification system, J. Appl. Meteorol., 43, 1834–1852, 2004.*

- *Horton, R.E. (1932): Drainage-basin characteristics. EOS Trans. Am. Geophys. Union 1932, 13, 350–361.*

- *Horton, R.E. (1945): Erosional development of streams and their drainage basins: hydrophysical approach to quantitative morphology. Bulletin of the Geological Society of America 56, 2 75-3 70.*

- *Hou, A. Y., Kakar, R. K., Neeck, S., Azarbarzin, A. A., Kummerow, C. D., Kojima, M., Oki R., Nakamura, K., and Iguchi, T., (2014): The Global Precipitation Measurement Mission, B. Am. Meteorol. Soc., 95, 701–722, 2014.*

- *Hsu, K., Gao, X., Sorooshian, S., and Gupta, H. V. (1997): Precipitation estimation from remotely sensed information using artificial neural networks, J. Appl. Meteorol. Clim., 36, 1176–1190.*

- *Karbalaee, N., Hsu, K., Sorooshian, S., and Braithwaite, D. (2017):*

Bias Adjustment of Infrared Rainfall Estimation Using Passive Microwave Satellite Rainfall Data, J. Geophys. Res.-Atmos., 122, 3857–3876.

- *Kavetski, D.; Kuczera, G.; Franks, S.W. (2006): Bayesian analysis of input uncertainty in hydrological modeling: 1. Theory. Water Resour. Res. 2006, 42.*
- *Kummerow, C., Barnes, W., Kozu, T., Shiue, J., and Simpson, J. (1998): The Tropical Rainfall Measuring Mission (TRMM) sensor package, J. Atmos. Ocean. Tech., 15, 809–817, 1998.*
- *Kummerow, C., Simpson, J., Thiele, O., Barnes, W., Chang, A. T. C., Stocker, E., Adler, R. F., Hou, A., Kakar, R., Wentz, F., Ashcroft, P., Kozu, T., Hong, Y., Okamoto, K., Iguchi, T., Kuroiwa, H., Im, E., Haddad, Z., Huffman, G., Ferrier, B., Olson, W. S., Zipser, E., Smith, E. A., Wilheit, T. T., North, G., Krishnamurti, T., and Nakamura, K. (2000): The status of the Tropical Rainfall Measuring Mission (TRMM) after two years in orbit, J. Appl. Meteorol., 39(12), 1965–1982, 2000.*
- *Meisner, B. N. and Arkin, P. A. (1987): Spatial and annual variation in the diurnal cycle of large-scale tropical convective cloudiness and precipitation, Mon. Weather Rev., 115, 1009–1032, 1987.*
- *Melton, M.A. (1957): An Analysis of the Relations among Elements of Climate, Surface Properties, and Geomorphology; Columbia University: New York, NY, USA, 1957.*
- *Michaelides, S.; Tymvios, F.; Michaelidou, T. (2009): Spatial and temporal characteristics of the annual rainfall frequency distribution in Cyprus. Atmos. Res. 2009, 94, 606–615.*
- *Miller, V.C. A (1953): Quantitative Geomorphic Study of Drainage Basin Characteristics in the Clinch Mountain Area, Virginia and Tennessee, Project nr:389-042, Technical Report 3; Columbia University: New York, NY, USA, 1953.*
- *Morisawa, M.E., (1985): "Rivers,form and Processes" , Longman,NewYork.*
- *Muller, E., (1974): Origins of Drumlins in Glacial Geomorphology, D.R.Cates (Ed.),Binghamton,New York , State Univ.*
- *Nguyen, P., Ombadi, M., Sorooshian, S., Hsu, K., AghaKouchak, A., Braithwaite, D., Ashouri, H., and Thorstensen, A. R. (2018): The PERSIANN family of global satellite precipitation data: a review*

and evaluation of products, Hydrol. Earth Syst. Sci., 22, 5801–5816.

- *Nguyen, P., Shearer, E., Tran, H. Ombadi, M., Hayatbini, N., Palacios, T., Huynh, P., Braithwaite, D., Updegraff, G., Hsu, K., Kuligowski, B., Logan, W., Sorooshian, S., (2019): The CHRS Data Portal, an easily accessible public repository for PERSIANN global satellite precipitation data. Sci Data 6, 180296.*
- *Sadeghi, M., Nguyen, P., Naeini, M, R., Hsu, K., Braithwaite, D., Sorooshian, S., (2021): PERSIANN-CCS-CDR, a 3-hourly 0.04° global precipitation climate data record for heavy precipitation studies. Sci Data 8, 157.*
- *Schumm, S.A., (1956): Evolution of drainage systems and slopes in badlands at Perth Amboy, New Jersey. Bull. Geol. Soc. Am. 67, 597–646.*
- *Schumm, S. A., (1977): The Fluvial system, John Wiley & Sons, New York.*
- *Scofield, R. A.: The NESDIS operational convective precipitation technique, Mon. Weather Rev., 115, 1773–1792, 1987.*
- *Smith, K.G., (1950): Standard for Grading Textures of Erosional Topography, Amer,Jour, Sci , Vol 248, p.p 651-675.*
- *Sorooshian, S., Hsu, K., Gao, X., Gupta, H. V., Imam, B., and Braithwaite, D. (2000): Evaluation of PERSIANN system satellite-based estimates of tropical rainfall, B. Am. Meteorol. Soc., 81, 2035–2046.*
- *Sorooshian, S., Gao, X., Hsu, K., Maddox, R. A., Hong, Y., Gupta, H. V., and Imam, B. (2002): Diurnal variability of tropical rainfall retrieved from combined GOES and TRMM satellite information, J. Climate, 15, 983–1001, 2002.*
- *Strahler, A.N., (1957): Quantitative Analysis of watershed Geomorphology Amer.Geophys. Union, Trans,38(6).*
- *Zhou, W., Tang, C., Van Asch, T.W.J., Chang, M., (2016): A rapid method to identify the potential of debris flow development induced by rainfall in the catchments of the Wenchuan earthquake area. Landslides 13, 1243–1259.*

استخدام تقديرات سقوط الأمطار المعتمدة على الأقمار الصناعية لرصد السيول بمنطقة وادي عربة غرب خليج السويس

ملخص:

توفر الصور الفضائية بيانات مهمة يمكن الاعتماد عليها لدراسة عناصر الطقس والمناخ من خلال الرصد المتكرر لهذه العناصر باستخدام أنظمة الاستشعار عن بعد التي تهتم بمثل هذه الأبحاث، مثل القمر الصناعي NOAA والذي يعتبر أقدم نظام للاستشعار المناخي عن بعد. تمثل الأقمار الصناعية أدلة لنماذج رياضية لتحديد توزيع الضغط وسمك درجة الحرارة وكثافة طبقات الغلاف الجوي، وحساب حركة الرياح بشكل غير مباشر عن طريق قياس حركة السحب من الأقمار الصناعية الثابتة، وكذلك استخدام التلسكوبات ذات القدرة العالية في المجالين البصري والحراري، كما أنها تسجل تدرج درجات الحرارة داخل طبقات السحب ومقارنتها وتستنتج نتائج أولية بسيطة. اعتمد هذا البحث على بيانات من مشروع تقدير هطول الأمطار من معلومات الاستشعار عن بعد باستخدام الشبكات العصبية الاصطناعية (PERSIANN) التابع لمركز مراقبة الأرصاد الجوية والهيدرولوجية والاستشعار عن بعد بجامعة كاليفورنيا والذي يعمل على استخلاص بيانات سقوط الأمطار من صور الأقمار الصناعية باستخدام نماذج الشبكة العصبية حيث تتوفر البيانات في أربعة أنماط تم الاعتماد من بينها نوع البيانات PERSIAN CCS على كونها بيانات مكانية دقيقة للغاية حيث تصل أبعاد الخلية إلى ٤ كم × ٤ كم. امتدت فترة البحث بين (٢٠١٥ – ٢٠٢١). خلال هذه الفترة تم تحليل هذه الملفات الرقمية ونمذجتها بغرض تحديد التغيرات المكانية والزمنية في سقوط الأمطار

المتوقعــة طــوال فتــرة الدراســة وتأثيراتهــا علــى الســيول فــي أحــواض منطقــة الدراســة. وكشـفت الدراسـة عـن تغيـر أنمـاط سـقوط الأمطـار، بمتوسـط ١٩.٨٥ ملــم فــي عــام ٢٠١٨ و٣.٨٣ ملــم فــي عــام ٢٠٢٠. وتلقــى الربيــع أعلــى معـدلات للأمطـار، حيـث بلـغ ١٧.٢٢ ملـم، يليـه الشـتاء بــ ١٤.٨٩ ملـم. شـهد شـهر مـارس أعلـى سقوط للأمطـار، حيـث بلـغ ١٩.٢ متـرًا، يليـه شـهر ديسـمبر بمعـدل ١٧.٧ متـرًا. وتـراوح حجـم السـيول فـي وادي عربـة مـن ٢٠٠ مليـون م٣ عامي ٢٠١٨ و٢٠١٩ إلى ١٠.٤١ مليون م٣ عام ٢٠١٥.

<u>الكلمـــــات المفتاحيـــــة:</u> تقــديرات هطــول الأمطــار – صــور الأقمــار الصناعية – السيول – وادي عربة.